RESEARCH ARTICLE

Quantification of the Atmospheric Corrosion of 304 and 2205 Stainless Steels Using Electrochemical Probes Based on Thevenin Electrochemical Equivalent Circuit Model

Yu Zhu[1,2] · Yang Song[1,2] · Likun Xu[3] · Zhenbo Qin[1,2] · Shizhe Song[1,2] · Wenbin Hu[1,2] · Da-Hai Xia[1,2]

Abstract

Stainless steel (SS) is one of the most widely used engineering materials in marine engineering. However, its corrosion in the marine atmospheric environment due to the high concentration of Cl^- is a problem. The SS corrosion is a threat to the development and security of marine industry; therefore, evaluating the corrosion resistance of SSs is necessary. In this work, atmospheric corrosion detection probes based on a symmetrical electrode system were used to study the corrosion behaviors of 304 SS and 2205 duplex stainless steel (DSS) in a simulated marine atmosphere. A theoretical model for electrochemical noise (EN) data analysis based on the Thevenin electrochemical equivalent circuit (EEC) model was established. The relationship between the EN characteristic parameters and the corrosion rate was obtained. The Thevenin EEC model analysis showed that the relationship between the noise resistance (R_n), the noise impedance [$R_{sn}(f)$], and the impedance modulus ($|Z(f)|$) was $R_n \approx R_{sn} = \sqrt{3}|Z(f)|$. Thus, R_n and R_{sn} can be used as indicators for quantitative corrosion evaluation. The results of EN detection for the 304 SS and 2205 DSS showed that in a simulated marine atmospheric environment, the passive films on the two SSs were relatively intact at the initial exposure stage, and their dissolution rates were slow. The corrosion resistance of the 2205 DSS was higher than that of the 304 SS. With the deposition of Cl^- on the SS surface, pitting was initiated and the dissolution rate increased. The pitting initiation process on the SS surface was random, and part of the active pores could be repassivated.

Keywords Atmospheric corrosion · Stainless steel · Electrochemical noise · Thevenin electrochemical equivalent circuit · Passive film

Introduction

The construction and maintenance of marine facilities is one of the key points to the sustainable development of the ocean. Metals are among the most important components of marine facilities. However, they are prone to pitting corrosion in Cl^--enriched environments, threatening the safety of

the facility. Thus, effective corrosion detection methods and maintenance measures are needed. The life-cycle maintenance of marine engineering facilities is of great significance to the economy and society, and corrosion detection is the basis of this maintenance.

Stainless steel (SS) is widely used in island facilities and military equipment such as ships [1, 2]. However, the atmospheric corrosion of SSs is an important factor restricting their applications. Therefore, developing an electrochemical method to detect the corrosion type and corrosion degree of metal materials is necessary. The electrochemical noise (EN) technique has been widely used in atmospheric corrosion detection because its detection equipment is simple and portable and can be used for remote continuous monitoring [3]. The application of EN technique requires proper data analysis [4–6], and the establishment of a reliable electrode system in the atmospheric environment [7, 8]. The data analysis of EN can represent the characteristic parameters of the corrosion type and corrosion

✉ Da-Hai Xia
dahaixia@tju.edu.cn

1 Tianjin Key Laboratory of Composite and Functional Materials, Tianjin 300354, China

2 School of Materials Science and Engineering, Tianjin University, Tianjin 300354, China

3 State Key Laboratory for Marine Corrosion and Protection, Luoyang Ship Material Research Institute (LSMRI), 149-1 Zhuzhou Road, Laoshan District, Qingdao 266101, China

degree of metal materials through time domain analysis, frequency domain analysis, and time–frequency analysis [9, 10].

Researchers around the world have applied the EN technique for corrosion detection. Sarmiento et al. [11] used EN to study the corrosion behavior of 316L SS at different temperatures in LiBr + ethylene glycol + H_2O solution and obtained the surface conditions and electrochemical behavior under corrosion conditions by EN measurement. Xia et al. [12] used EN to monitor the atmospheric corrosion of Q235B steel, quantified the corrosion rate using statistical parameters and frequency domain analysis, and evaluated the reliability of EN measurement coupled with electrochemical impedance spectroscopy. Pujar et al. [13] verified that EN could evaluate the intergranular corrosion of 316 SS. Tang et al. [14] studied the influence of surface roughness on the pitting behavior of 2205 DSS in a Cl^- environment by EN measurement and morphological observation. However, some of the mathematical parameters lack strict physical meaning; thus, it is very important to conduct electrochemical equivalent circuit (EEC) analysis in order to further study the physical meaning of EN feature parameters and influencing factors. In addition, the corrosion of metal materials in the solution environment has been well documented, but the corrosion in the atmospheric environment has rarely been investigated. As the solution resistance varies greatly with different environments and times due to humidity, pollutant composition, and other factors, the detection results will be largely affected. Therefore, establishing an EEC model for EN data analysis of metal corrosion in the atmospheric environment is necessary. Moreover, the influence of solution resistance on EN characteristic parameters, such as the power spectral density (PSD) of potential noise, the PSD of current noise, noise impedance, and noise resistance also needs to be examined.

This study investigated the atmospheric corrosion of 304 SS and 2205 DSS using EN in a simulated marine atmosphere, clarified the factors affecting the EN characteristic parameters, and obtained the corrosion rate based on the Thevenin EEC model. Atmospheric corrosion probes of 304 SS and 2205 DSS were developed, and EN detection was performed under a salt spray containing Cl^- in a dry–wet cycle test. The original EN data were analyzed in time and frequency domains. In addition to analyzing the surface morphology, the corrosion degrees of 304 and 2205 SSs under the same atmospheric environment were evaluated.

Experimental Procedures

Electrochemical Probes

Two electrochemical probes were used to study the atmospheric corrosion of 304 and 2205 SSs. One of their schematic diagrams is shown in Fig. 1. The probe incorporates three identical electrodes made by 304 or 2205 SS, with an exposure area of 0.75 cm^2 for each electrode. This type of setup is called a symmetrical electrode system [15–18]. The experimental materials are 304 SS and 2205 DSS. Their chemical components are presented in Table 1, and their microstructures are shown in Fig. 2. The 304 SS is austenitic, whereas the 2205 DSS is composed of ferrite and austenite.

To isolate the three electrodes, a gap of 0.2 mm existed between the adjacent electrodes [12, 19], as shown in Fig. 1. The three electrodes were embedded in an epoxy resin. The working face was polished with waterproof abrasive papers of 400#, 800#, 1200#, 1500#, and 2000#, and the non-exposed area of each electrode was welded to a copper wire, to connect the electrochemical measurement system.
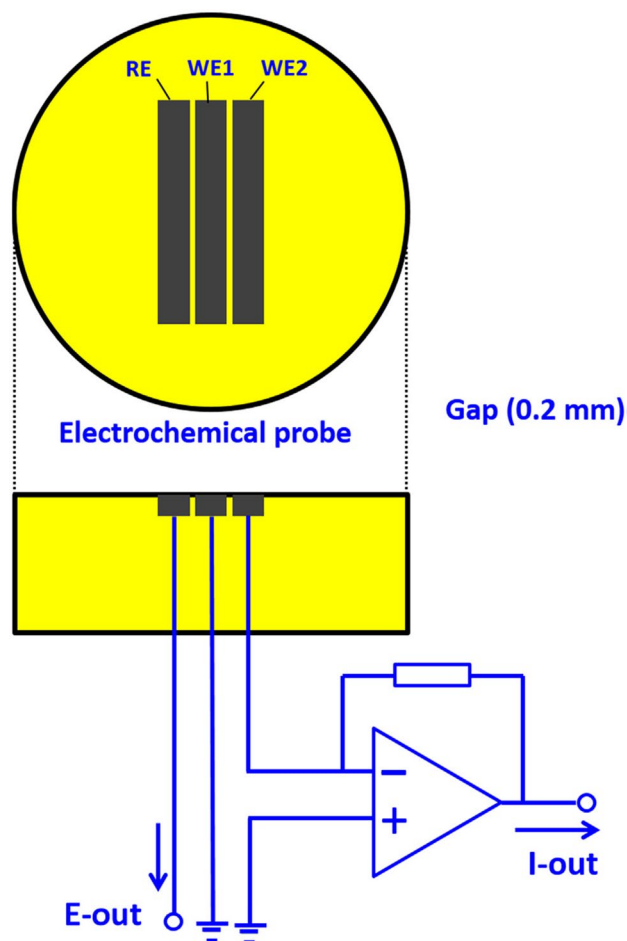
Fig. 1 Schematic diagram of atmospheric corrosion probe and the electric schematic diagram for electrochemical noise measurement

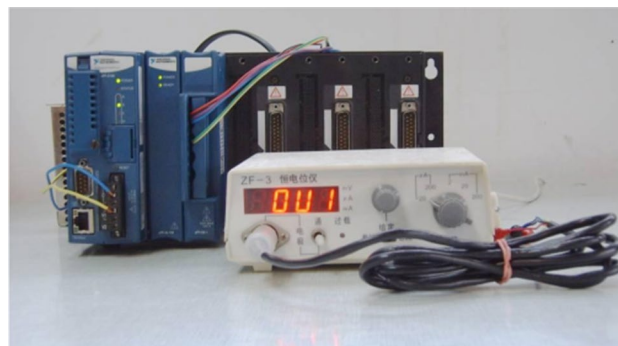**Table 1** Chemical compositions of 304 SS and 2205 DSS (wt%)

Materials	C	Si	Mn	P	S	Cr	Ni	Mo	Fe
304 SS	0.08	1.00	2.00	0.045	0.030	18.0	10.0	–	Balance
2205 DSS	0.014	0.39	1.38	0.023	0.001	22.39	5.68	3.00	Balance
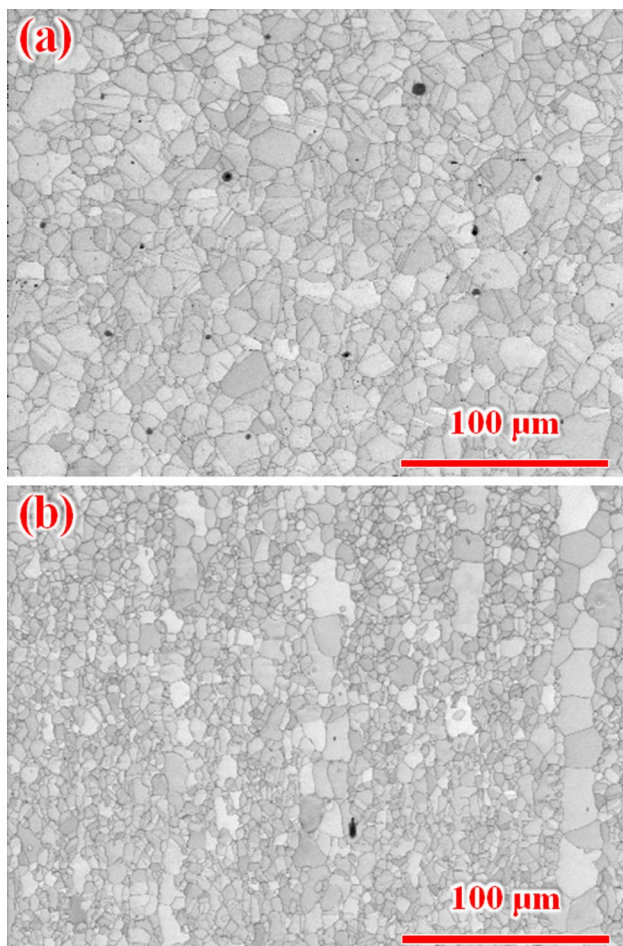
Fig. 2 Microstructures of **a** 304 SS and **b** 2205 DSS

Fig. 3 Electrochemical noise detection system based on the Field-Point analog input module cFP-AI-118 NI, a ZF3 potentiometer, and a Compact FieldPoint industrial controller module

EN Measurement System and Experiment

The two 304 SS and 2205 DSS probes were placed in a salt spray environment, which was filled with atomized 5% NaCl solution to simulate the marine atmosphere. Each probe surface was tilted 45° to the horizontal plane for the dry–wet cycle test. One cycle period was 4 h, including 2 h wetting time with experimental temperature of 50 °C and 2 h drying time with experimental temperature of 35 °C.

The EN measurement was conducted by a system composed of the FieldPoint analog input module CFP-AI-118 NI, a ZF3 potentiometer, and a Compact FieldPoint (CFP) industrial controller module (Fig. 3). The zero resistance ammeter (ZRA) mode was adopted for detection, and the sampling frequency was 2 Hz [6, 20]. The DC components in all the EN data were removed using a quintic polynomial fitting [21–23].

Electrochemical Equivalent Circuit Model

The Thevenin EEC proposed by Bertocci et al. [24] is one of the most commonly used methods for modeling EN sources. First, the effectiveness of the electrochemical parameters measured by EN in the ZRA mode to test the SS corrosion degree should be determined. The electrochemical parameters include potential standard deviation, current standard deviation, and noise resistance [25, 26].

The atmospheric corrosion detection probes for EN measurement at the 304 SS and 2205 DSS consisted of three identical SS electrodes, all of which generate potential or current noise. The EEC models are shown in Fig. 4a, b. In the figures, WE1 in the middle denotes the working electrode, WE2 on the right denotes the counter electrode, and RE on the left is the reference electrode.

Since the three electrodes are nominally identical, the noise impedance $R_{sn}(f)$ is equal to $\sqrt{3}|Z(f)|$ [24, 25], and the noise resistance R_n is equal to the low frequency limit of $R_{sn}(f)$ for some assumptions [24]. Therefore, R_n and $R_{sn}(f)$ are related only to the electrode impedance modulus $|Z(f)|$ and can be used as indicators to evaluate the atmospheric corrosion degree.
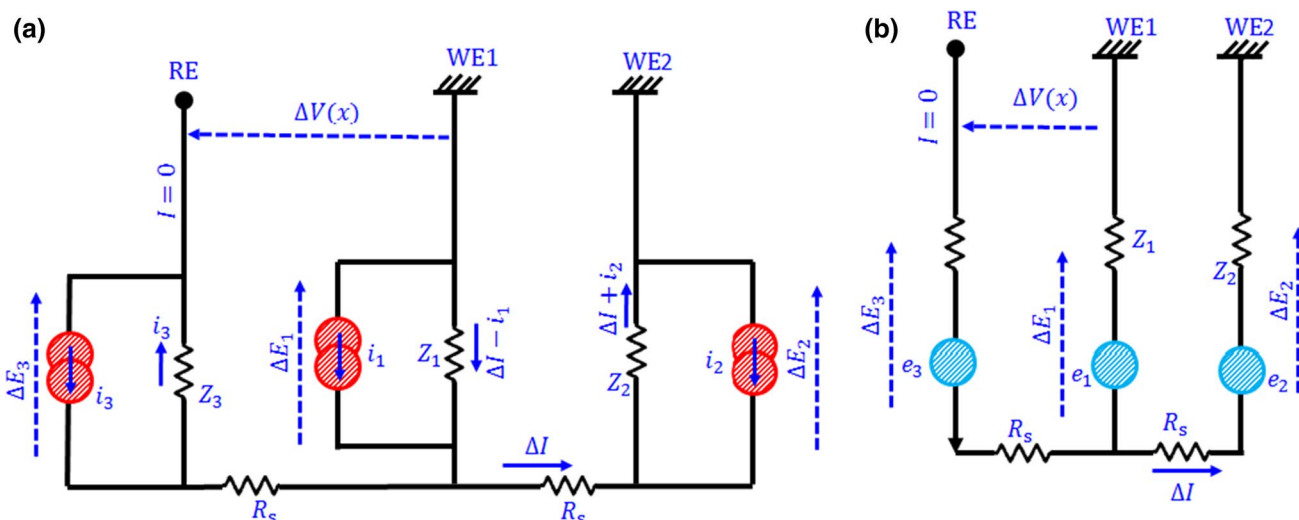
Fig. 4 Equivalent circuit model of the atmospheric corrosion detection probe with three identical electrodes used in EN test. **a** Equivalent circuit for current noise and **b** equivalent circuit for potential noise

## Results and Discussion

EN Time Domain Analysis

Figures 5 and 6 show the current noise and potential noise after removing the DC component for the 304 SS and 2205 DSS, respectively, during dry–wet cycle EN measurements. The potential standard deviation, current standard deviation, and noise resistance of the two SSs are presented in Tables 2 and 3, respectively. The results showed that at the beginning, the current noise fluctuation of the two SSs was small (Figs. 5a, 6a), indicating that the

passive film on the SS surface was intact, and the corrosion rate was slow. The potential noise fluctuated greatly, possibly because the surface state of the SS was unstable after a brief exposure to the Cl^--containing atmosphere.

As the number of dry–wet cycles increased (Figs. 5b, 6b), Cl^- kept depositing on the SS surface; a stable state was gradually reached, and the potential standard deviation decreased. At this stage, synchronous transient peaks began to appear on the potential and current noise curves, the standard deviation of current increased, and the noise resistance decreased. This is due to Cl^--induced corrosion, which led to the rupture and repair of the passive film on the SS surface, pitting initiation, and corrosion rate increase. The
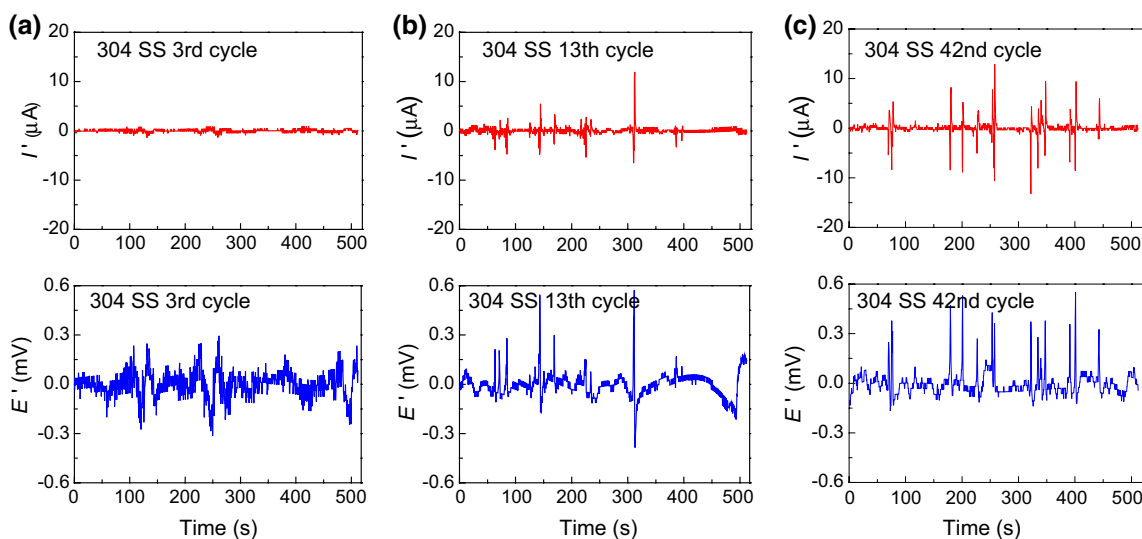
Fig. 5 Current noise and potential noise of 304 SS. **a** The third cycle, **b** the 13th cycle, and **c** the 42nd cycle
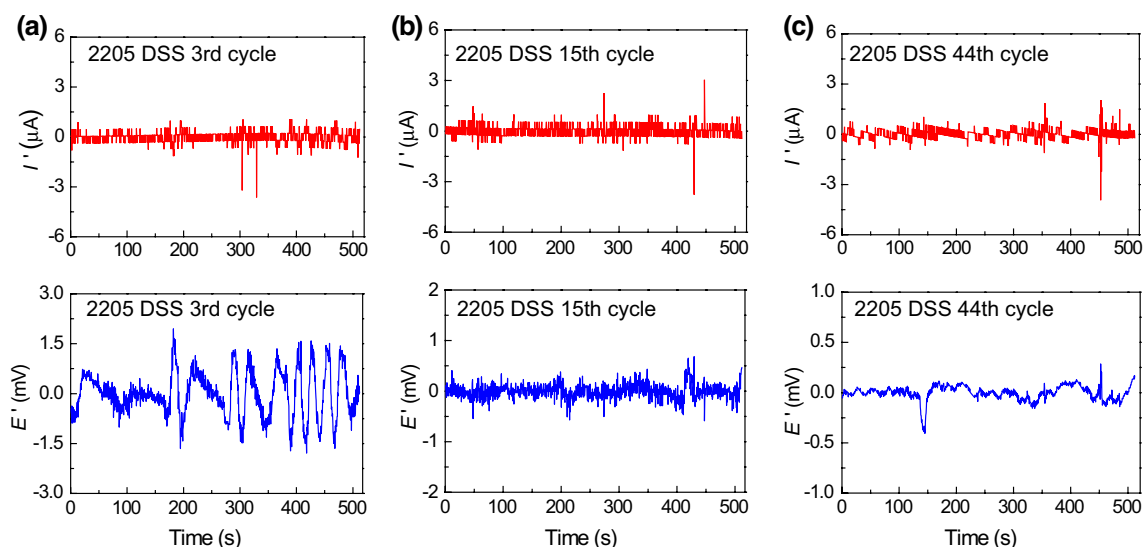
Fig. 6 Current noise and potential noise of 2205 DSS. **a** The third cycle, **b** the 15th cycle, and **c** the 44th cycle

Table 2 Fitted electrochemical parameters of EN detection for 304 SS
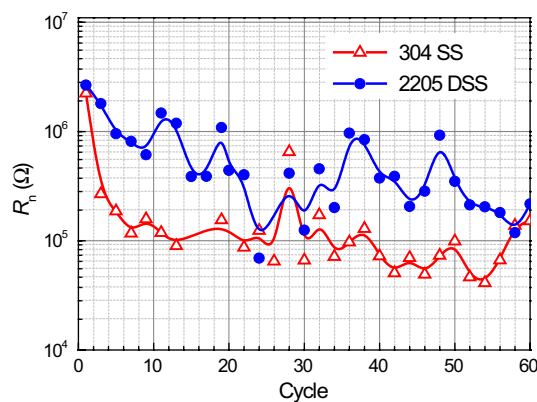
Dry–wet cycle number	E' (mV)	I' (μA)	R_n (Ω)
304-3rd cycle	0.0801515	0.298564	268582.16
304-13th cycle	0.0756261	0.910745	83037.57
304-42nd cycle	0.0776160	0.152923	50754.78

Table 3 Fitted electrochemical parameters of EN detection for 2205 DSS

Dry–wet cycle number	E' (mV)	I' (μA)	R_n (Ω)
2205-3rd cycle	0.6787850	0.377680	1797248.13
2205-15th cycle	0.1490090	0.385259	386777.13
2205-44th cycle	0.0723677	0.351169	206076.79

Fig. 7 Noise resistances of 304 SS and 2205 DSS EN detection

results show that the pitting initiation on the SS surface did not propagate all the time; it can repassivate. At the initial stage when the passive film was damaged, the effect on the stability of the passive film was little. The pitting initiation in each dry–wet cycle was random and characterized by low probability. The pits can also be repaired again.

After over 40 dry–wet cycle tests, the fluctuations of current noise and potential noise on the 304 SS (Fig. 5c) increased, and a large number of transient peaks appeared simultaneously. At the same time, the standard deviations of current and potential increased, indicating that the damage degree of the passive film further increased, the probability of pitting increased, and the corrosion rate increased. However, the fluctuations of current noise and potential noise on the 2205 DSS (Fig. 6c) were still lower than those on the 304

SS. Moreover, the standard deviation of current, the standard deviation of potential, and the noise resistance were not significantly changed, which indicates that the passive film on the 2205 DSS surface was still complete, and the resistance to Cl⁻ corrosion was more than that of the 304 SS.
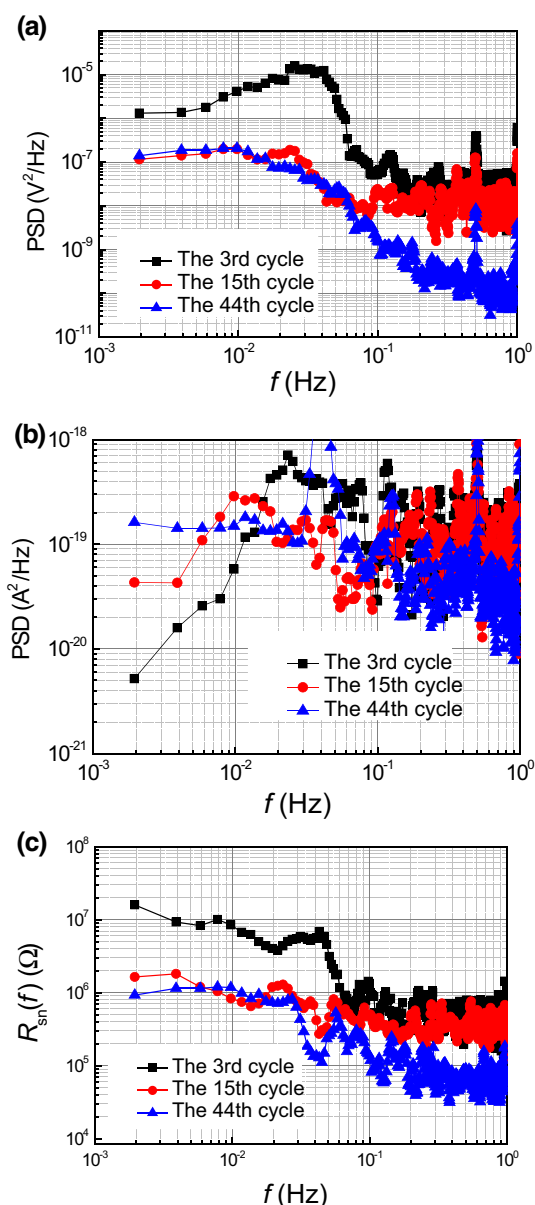
The noise resistances of 304 SS and 2205 DSS during the dry–wet cycle EN measurement are depicted in Fig. 7. The noise resistance is only related to the impedance modulus of the electrode and can be used as an indicator to evaluate the atmospheric corrosion degree. At the beginning of the dry–wet cycle test, both the 304 SS and 2205 DSS featured high noise resistance, indicating that the passive film on the SS surface was complete, strong resistance to Cl⁻-induced corrosion, and a low corrosion rate. As the number of dry–wet cycles increased, the noise resistances of both SSs were reduced, indicating that the passive film broke and pitting began to occur. However, the resistance did not decrease
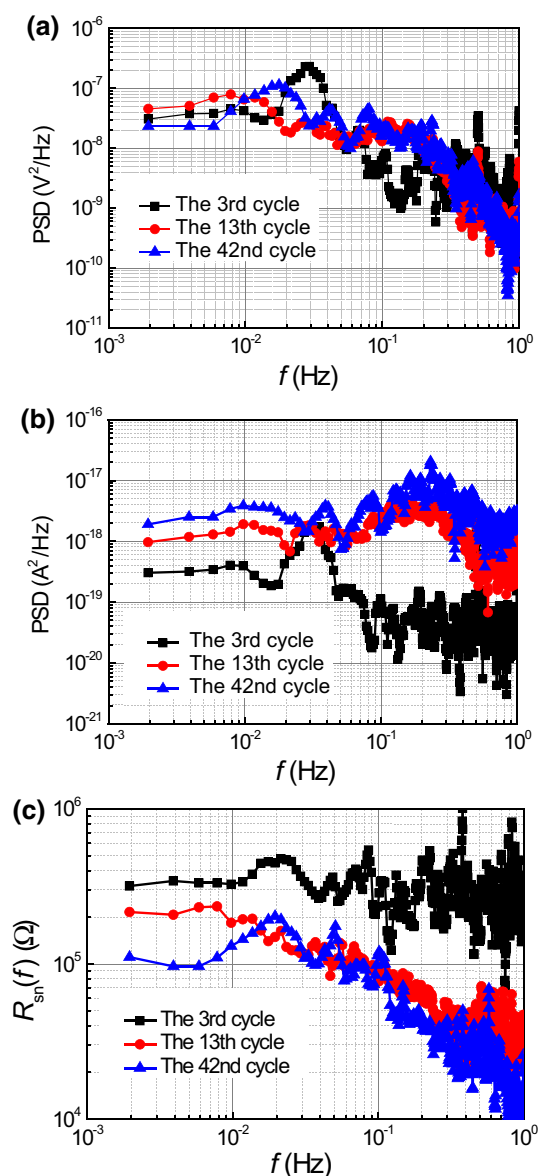
Fig. 8 Frequency domain analysis results of the 304 SS EN data as shown in Fig. 5. **a** Power spectral density of potential noise, **b** power spectral density of current noise, and **c** noise impedance

Fig. 9 Frequency domain analysis results of the 2205 DSS EN data as shown in Fig. 6. **a** Power spectral density of potential noise, **b** power spectral density of current noise, and **c** noise impedance

steadily but alternated between decreasing and increasing, which also proved that the SS passive film will be repaired after being broken, and the pitting will still be passivated during the next dry–wet cycle.

Although the noise resistances of the 304 SS and 2205 DSS maintained a high order of magnitude in the experiments, indicating a better corrosion resistance and lower corrosion rate, they both decreased with increasing the number of dry–wet cycles. It shows that even at the pitting initiation stage, pits can be repassivated, but continuous pitting still

has a destructive effect on the passive film. As this minor damage accumulated, the SS gradually became less resistant to Cl^--induced corrosion, and the corrosion rate increased, eventually leading to the failure of the SS.

The noise resistances of 304 SS and 2205 DSS are about 10^5 and 10^6 Ω, respectively. Even though the noise resistance is reduced overall, the latter is still an order of magnitude higher than the former, indicating that the 2205 DSS has a
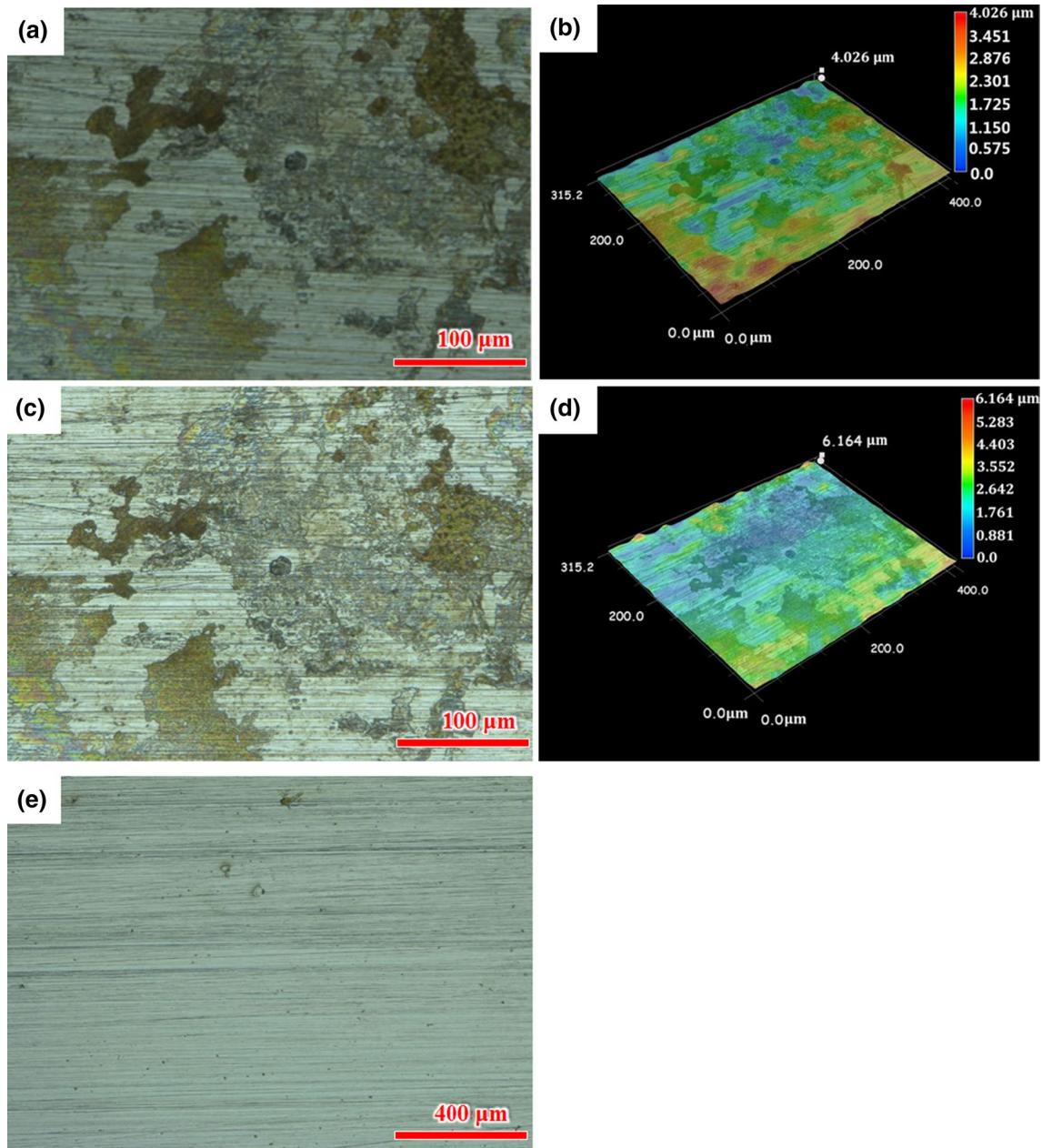
Fig. 10 Surface morphology of 304 SS. **a** 2D image after 25 cycles, **b** 3D image after 25 cycles, **c** 2D image after 60 cycles, **d** 3D image after 60 cycles, and **e** enlarged 2D image after 60 cycles

better corrosion resistance. The high corrosion resistance of DSS is due to its high-Cr content and a large amount of Mo, Ni, and N elements. Chromium can form a protective passive film of Cr–O/OH on the DSS surface. The synergistic effect between Cr and Mo–O/OH improves the DSS pitting stability. Nitrogen acts as a kind of interstitial solid solution element to enhance the DSS tensile properties.

Frequency Domain Analysis

Figure 8 depicts the frequency domain analysis results of the 304 SS EN data as shown in Fig. 5. As the number of dry–wet cycles increased, the PSDs of potential noise and noise impedances decreased, while the PSDs of current noise increased. This indicates that with the increase

in pitting corrosion on the 304 SS surface, the passive film was increasingly destroyed, the SS corrosion resistance decreased, and the corrosion rate increased as well.

Figure 9 shows the frequency domain analysis results of the 2205 DSS EN data as shown in Fig. 6. As the number of dry–wet cycles increased, the PSDs of potential noise and noise impedances decreased, while the PSDs of current noise increased and then tended to stabilize. This indicates that with the development of the experiment, pitting corrosion occurred on the 2205 DSS surface, the passive film broke down, and the SS corrosion resistance decreased. However, the passive film on the 2205 DSS was stable and complete in the initial exposure stage. The 2205 DSS exhibited a better corrosion resistance compared with the 304 SS under the same experimental conditions.

Morphology Analysis

A KEYENCE VHX-2000C ultra-depth 3D microscope was used to observe the surface morphology of corroded samples. Figure 10 shows the surface morphology of a pitting location of the 304 SS after 25 and 60 dry–wet cycles. After 25 cycles, the pits were very small and had a depth of less than 5 μm, but many corrosion products occurred around the pits. After 60 cycles, the morphology of the pitting location changed little, and the pitting did not expand in depth or radius. Figure 10e shows the microscopic surface morphology under a 3D microscope after 60 cycles. It can be seen that a large number of micron-scale pits appeared on the SS surface. This confirms that the rupture and pitting initiation of the passivated film on the SS surface were random. The location of each pitting may not be the same as that of the last one. The non-expansion of the pitting hole also indicates that the passive film can be repaired after the rupture, and the pitting location still featured good corrosion resistance after the passivation.

Figure 11 shows the surface morphology of a pitting location of the 2205 DSS after 25 and 60 dry–wet cycles. Only a few corrosion products covered the surface, and the pits were too small to be observed in the figure. Moreover, most areas of the sample surface were smooth, with only a few tiny pits (Fig. 11c).

After 60 cycles, the macromorphology of 304 SS and 2205 DSS changed little, and the surface was bright. However, using a 3D microscope, a large number of tiny pitting holes could be observed on the 304 SS. It indicates that under normal service conditions, the large number of tiny pits on the 304 SS surface can hardly be noticed, but their existence will significantly reduce the 304 SS corrosion resistance. Therefore, the material should be tested and maintained on time to avoid premature failure. The 2205 DSS surface featured few micro-erosion holes, and the depth
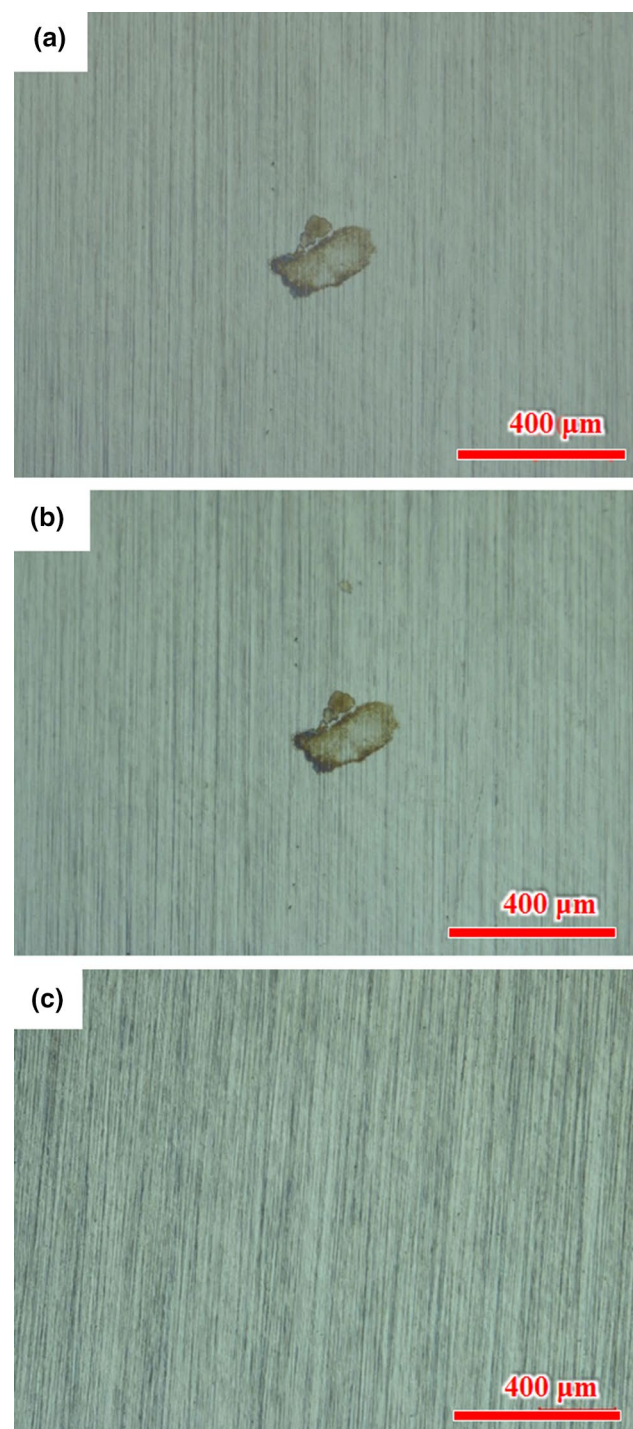
Fig. 11 Surface morphology of the 2205 DSS. **a** After 25 cycles, **b**, and **c** two different areas after 60 cycles

and radius of the pitting holes were much smaller than those of the 304 SS. This indicates that the corrosion resistance of 2205 DSS is much better than that of 304 SS under the same working conditions.

Conclusions

In this article, the atmospheric corrosions of 304 SS and 2205 DSS were investigated using the EN technique, and the results are summarized as follows:

(1) All three 304 or 2205 SS electrodes in the probes produced current noise and potential noise, which could be detected using the EN technique. When the three electrodes have the same impedance modulus $|Z(f)|$, then we have $R_{sn}(f) = \sqrt{3}|Z(f)|$; thus, R_n and R_{sn} can be used as indicators to evaluate atmospheric corrosion degree.

(2) At the initiation of the dry–wet cycle experiment, the SS passive film was intact, and its dissolution rate was low.

(3) As the number of dry–wet cycles increased, Cl^- was deposited on the SS surface and broke the passive film, pitting was initiated, and the corrosion rate increased. Under the same experimental conditions, the 2205 DSS exhibited better corrosion resistance than the 304 SS.

(4) The pitting initiation of the passivated film on the SS surface was random. At the initial stage of the experiment, the pitting location still had good corrosion resistance after the passivation.

(5) With the pitting corrosion propagation, the corrosion resistance was persistently reduced for the two SSs.

References

1. Pan C, Song Y, Jin W et al (2020) Enhancing the stability of passive film on 304 SS by chemical modification in alkaline phosphate-molybdate solutions. Trans Tianjin Univ. https://doi.org/10.1007/s12209-020-00238-8
2. Xia DH, Sun YF, Fan HQ (2015) Characterization of passive film formed on 304 SS in simulated alkaline water chemistries containing sulphur at 300 °C. Trans Tianjin Univ 21(6):554–561
3. Xia DH, Ma C, Song SZ et al (2017) Assessing atmospheric corrosion of metals by a novel electrochemical sensor combining with a thin insulating net using electrochemical noise technique. Sens Actuators B Chem 252:353–358
4. Xia DH, Song SZ, Behnamian Y (2016) Detection of corrosion degradation using electrochemical noise (EN): review of signal processing methods for identifying corrosion forms. Corros Eng Sci Technol 51(7):527–544
5. Zhang T, Yang YG, Shao YW et al (2014) Advances of the analysis methodology for electrochemical noise. J Chin Soc Corros Prot 34:1–18 **(in Chinese)**
6. Monrrabal G, Huet F, Bautista A (2019) Electrochemical noise measurements on stainless steel using a gelled electrolyte. Corros Sci 148:48–56
7. Xia D, Song S, Li J et al (2017) On-line monitoring atmospheric corrosion of metal materials by using a novel corrosion electrochemical sensor. Corros Sci Prot Technol 29:581–585 **(in Chinese)**
8. Ritter S, Huet F, Cottis RA (2012) Guideline for an assessment of electrochemical noise measurement devices. Mater Corros 63(4):297–302
9. Homborg AM, Tinga T, van Westing EPM et al (2014) A critical appraisal of the interpretation of electrochemical noise for corrosion studies. Corrosion 70(10):971–987
10. Cottis RA, Homborg AM, Mol JMC (2016) The relationship between spectral and wavelet techniques for noise analysis. Electrochim Acta 202:277–287
11. Sarmiento E, Uruchurtu J, González-Rodriguez JG et al (2011) Electrochemical noise analysis of type 316L stainless steel in a LiBr + ethylene glycol + H$_2$O solution. Corrosion 67(10):105004
12. Xia DH, Ma C, Behnamian Y et al (2019) Reliability of the estimation of uniform corrosion rate of Q235B steel under simulated marine atmospheric conditions by electrochemical noise (EN) analyses. Measurement 148:106946
13. Pujar MG, Parvathavarthini N, Dayal RK et al (2009) Assessment of intergranular corrosion (IGC) in 316(N) stainless steel using electrochemical noise (EN) technique. Corros Sci 51(8):1707–1713
14. Tang YW, Dai NW, Wu J et al (2019) Effect of surface roughness on pitting corrosion of 2205 duplex stainless steel investigated by electrochemical noise measurements. Materials 12(5):738
15. Bahrami MJ, Shahidi M, Hosseini SMA (2014) Comparison of electrochemical current noise signals arising from symmetrical and asymmetrical electrodes made of Al alloys at different pH values using statistical and wavelet analysis. Part I: neutral and acidic solutions. Electrochim Acta 148:127–144
16. Cottis RA (2007) The significance of electrochemical noise measurements on asymmetric electrodes. Electrochim Acta 52(27):7585–7589
17. Bosch RW, Cottis RA, Csecs K et al (2014) Reliability of electrochemical noise measurements: results of round-robin testing on electrochemical noise. Electrochim Acta 120:379–389
18. Xia DH, Song SZ (2019) Development of theoretical models regarding with electrochemical noise applied in corrosion rate measurement. CIESC J 70:3880–3891 **(in Chinese)**
19. Xia DH, Song SZ, Qin ZB et al (2020) Review: electrochemical probes and sensors designed for time-dependent atmospheric corrosion monitoring: fundamentals, progress, and challenges. J Electrochem Soc 167(3):037513
20. Huet F, Ngo K (2019) Electrochemical noise: guidance for improving measurements and data analysis. Corrosion 75(9):1065–1073
21. Bertocci U, Huet F, Nogueira RP et al (2002) Drift removal procedures in the analysis of electrochemical noise. Corrosion 58(4):337–347

22. Xia DH, Behnamian Y (2015) Electrochemical noise: a review of experimental setup, instrumentation and DC removal. Russ J Electrochem 51(7):593–601

23. Cottis RA (2001) Interpretation of electrochemical noise data. Corrosion 57(3):265–285

24. Bertocci U, Gabrielli C, Huet F et al (1997) Noise resistance applied to corrosion measurements: I. Theoretical analysis. J Electrochem Soc 144:31–37

25. Xia DH, Ma C, Song SZ et al (2019) Detection of atmospheric corrosion of aluminium alloys by electrochemical probes: theoretical analysis and experimental tests. J Electrochem Soc 166(12):B1000–B1009

26. Meng FD, Liu YS, Liu L et al (2019) Effect of asymmetric epoxy coating/metal electrodes on the electrochemical noise measurements under marine alternating hydrostatic pressure. Coatings 9(12):852

Da-Hai Xia is a teacher at the School of Materials Science and Engineering, Tianjin University. He received his Ph.D. degree from Tianjin University (China) in 2012, and then joined the postdoctoral fellowship (2013–2014) at the University of Alberta (Canada) under the guidance of Prof. Jing-Li Luo. His research interests are interdisciplinary studies of corrosion, electrochemistry, and surface science.